Tsaimou *et al*. *Complex Eng Syst* 2024;4:20
DOI: 10.20517/ces.2024.28

Complex Engineering Systems

Research Article

Open Access

Mapping cracks on port concrete pavements by analyzing structural health monitoring metadata with computer vision-based techniques

Christina N. Tsaimou[1], Georgios Kagkelis[1], Panagiotis Sartampakos[2], Konstantinos Karantzalos[3], Vasiliki K. Tsoukala[1]

[1]Laboratory of Harbour Works, Department of Water Resources and Environmental Engineering, School of Civil Engineering, National Technical University of Athens (NTUA), Zografou 15780, Greece.
[2]NIREAS Engineering, 8 Katsikogianni Str., Chalkida 34100, Greece.
[3]Remote Sensing Laboratory, School of Rural, Surveying and Geo-Informatics Engineering, National Technical University of Athens (NTUA), Zografou 15780, Greece.

Correspondence to: Christina N. Tsaimou, Laboratory of Harbour Works, Department of Water Resources and Environmen-tal Engineering, School of Civil Engineering, National Technical University of Athens (NTUA), Zografou 15780, Greece. E-mail: ctsaimou@gmail.com; Prof. Vasiliki K. Tsoukala, Laboratory of Harbour Works, Department of Water Resources and Environmental Engineering, School of Civil Engineering, National Technical University of Athens (NTUA), Zografou 15780, Greece. E-mail: tsoukala@mail.ntua.gr

How to cite this article: Tsaimou CN, Kagkelis G, Sartampakos P, Karantzalos K, Tsoukala VK. Mapping cracks on port concrete pavements by analyzing structural health monitoring metadata with computer vision-based techniques. *Complex Eng Syst* 2024;4:20. http://dx.doi.org/10.20517/ces.2024.28

Received: 7 Jun 2024 **First Decision:** 29 Aug 2024 **Revised:** 14 Oct 2024 **Accepted:** 8 Nov 2024 **Published:** 14 Nov 2024

Academic Editor: Hamid Reza Karimi **Copy Editor:** Fangling Lan **Production Editor:** Fangling Lan

Abstract

Ports act as hubs for international trade and transport, strengthening the economies of the regions they serve. To maintain their undisrupted operations, efficient port management systems rely on Structural Health Monitoring practices to detect defects and assess infrastructure performance. Regarding port concrete pavements, condition assessment includes crack detection. Currently, advanced algorithms and methodologies for image processing or machine learning applications are used for surface crack detection with images captured during *in-situ* inspections. The growing urge to employ unmanned aerial vehicles (UAVs) equipped with high-resolution cameras is driving further research into image processing methods. This study provides an insightful approach for real-time crack detection in port concrete pavements that takes advantage of the geospatial information included in UAV imagery. The proposed methodology is based on the synergetic application of programming and Geographic Information System tools. Widely used crack detection methods and algorithms are herein enhanced with geospatial analysis modules that help to manage photogrammetry metadata generated by processing UAV data. Geographic Information System tools are employed to

add a new perspective to crack detection by supporting the visualization and interpretation of geospatial processed images to locate cracks and examine crack propagation. The investigation includes a periodic field test conducted at Lavrio Port, a Greek port located at the southeastern tip of Attica. Overall, the combined methodology returns results with high accuracy (approximately 95%), thus having a practical application in the engineering community that shifts to scalable solutions for mapping cracks in large port concrete surfaces remotely inspected with UAVs.

Keywords: Port pavements, port concrete infrastructure, structural health monitoring (SHM), condition assessment, unmanned aerial vehicles (UAVs), crack detection, image analysis, geographic information systems (GIS)

1 INTRODUCTION

Ports are key nodes having a dynamizing effect on trade, maritime connectivity and transportation, logistics chain, and the blue economy[1]. They are capital-intensive infrastructure assets whose performance is disturbed by natural disasters (e.g., earthquakes and storms), human-induced threats (e.g., human accidents), adverse marine conditions, and climate change impact[2,3],necessitating continuous maintenance and upgrade actions[4–6]. To implement a proactive intervention plan, optimize maintenance resources, and enhance the structural integrity of port infrastructure, port managers are tasked to establish effective asset management programs[7].

Nowadays, Structural Health Monitoring (SHM) of infrastructure is gaining importance in asset management[6,8]. Within the port industry, SHM of constructed port concrete facilities can be measured using an index that requires structural condition data linked to cracking, spalling, corrosion, and other defects[4]. Cracking in port concrete pavements of mooring facilities is often caused by traffic loading conditions (e.g., loading from heavy truck vehicles), inadequate design, construction defects, humidity conditions, *etc.*[9]. Crack detection in such facilities is essential to retain structural and functional performance, ensure public safety, reduce maintenance costs, and prevent operational delays associated with non-targeted repair interventions[9,10].

Computer vision-based techniques for SHM of concrete structures have gained rapid popularity in terms of crack detection[4]. They include both processing-based (i.e., image processing) and learning-based (i.e., deep learning) techniques[11,12]. Digital Image Processing (DIP) is widely used to apply crack detection on concrete surfaces aiming at enhancing the procedures of assessing existing condition[12]. DIP is applied with several methodologies that involve data collection, data pre-processing, and algorithms' implementation for crack detection. Imagery acquisition involves both manual (e.g., handheld cameras) or automated applications (e.g., cameras mounted on Unmanned Aerial Vehicles, UAVs)[10]. The latter can be extremely beneficial for structures that occupy large areas, e.g., the port concrete pavements of mooring facilities, where limited handheld photography may not representatively illustrate the *in-situ* condition of such infrastructure.

Current literature identifies the need to integrate UAV datasets into crack detection practices. The unique characteristics of images captured by cameras mounted on UAVs such as resolution, lighting conditions, image distortion, capturing distance, and lens' characteristics differ from those taken with handheld cameras[13,14]. Hence, different studies have been focused on developing methods for crack detection by adapting to the requirements of analyzing UAV datasets. For example, approaches for pixel-level crack identification[15] and noise reduction[16] have been investigated. Despite the ever-increasing interest in crack detection using UAV imagery, as noted by[17], few studies have focused on localizing cracks in concrete structures with UAV-collected images. In the specific study, the localization was achieved by considering the relative position between objects. Another study focused on locating cracks in the world coordinate system using two UAV-based images[18]. However, the potential of geospatial information in large UAV datasets required to illustrate large structures remains largely untapped.

The growing trend of UAV-driven SHM of port concrete pavements assists in identifying cracks in geospatial output produced by photogrammetry methods and inserted into Geographic Information Systems (GIS)[19]. GIS tools have proven to be promising for manually mapping cracks albeit the lack of engaging automated or semi-automated approaches for crack detection. Although advancing automation in crack detection with coding for image processing and deep learning techniques has occupied several researchers, the synergetic application of programming and GIS tools has not yet been explored. Programming languages can be used to implement algorithms for crack detection[20] while GIS tools allow for managing the geospatial information[21] included in orthophotos that are generated by analyzing UAV imagery. Hence, interrelating both approaches can be quite compelling in terms of assisting an SHM program for port concrete pavements. Except for combining programming and GIS tools for concrete crack detection, proposed practices included in existing works are not tested on UAV imagery acquired on different dates thus searching for changes in crack propagation. While ensuring a reliable output in crack detection is very important, within the framework of civil engineering applications a comprehensive understanding of structural changes is also crucial for managing maintenance interventions.

In light of the above, the present research seeks to contribute to the existing body of knowledge regarding automating crack detection on port concrete pavements by applying current practices in image analysis enhanced with tools for working with geospatial information. Such tools include (a) modules imported in programming languages for managing georeferenced images; and (b) GIS applications for analyzing geospatial metadata acquired by image analysis. The proposed methodology is applied at Lavrio Port, located in the southeastern tip of Attica, Greece. The investigation includes a periodic SHM scheme that encompasses four UAV-based in-situ inspections (ISIs), photogrammetry analyses, python coding, and GIS applications, thus providing a comprehensive outline for facilitating crack detection issues.

To examine the synergistic effect of crack detection algorithms and geospatial tools on advancing structural condition assessment of port concrete pavements, the paper is organized as follows. The current background on crack detection practices is firstly summarized in Section 2 by describing pioneering contributions to algorithm development and later-triggered works. Based on the existing framework a structured methodology is presented that initiates a real-time crack detection approach that utilizes geospatial information of UAV orthophotos to map cracking on port concrete slabs of mooring facilities. The methodology is applied at a pilot area defined within a concrete slab of the domestic ferry mooring facilities of Lavrio port to test its applicability. The analysis of the results [Section 3] includes data validation and change detection during ISIs. The most significant issues noticed while working on the specific case study are further discussed aiming to identify challenges and search for potential ways to address them [Section 4]. Finally, the major findings of the demo application are enclosed in Section 5.

2 MATERIALS AND METHODS

2.1 Background and objectives

UAVs are usually equipped with high-resolution Ultra 4K cameras for capturing digital aerial images[22]. In contrast to the processing of imagery captured with portable cameras, where crack detection can be localized, the analysis of UAV imagery of port concrete infrastructure is compromised by the presence of noise features[16,23]. This is due to the complexity of the surrounding conditions including the shadows of vehicles and passengers, linear joints, manholes, and other defects such as spalling and corrosion. To address these challenges, several scientists have turned their research to deep learning techniques for machine learning applications[24] aiming to classify and recognize cracks with pre-trained algorithms. The efficiency of such techniques is highly dependent on the amount of available imagery and the quality of the representative training dataset. Indicatively, both seasonal and daily time variations in UAV-captured images, the presence of wet pavements, lighting conditions of the sun, and the cracking pattern (e.g., diagonal, transverse, longitudinal,

wide/narrow cracks, *etc.*) may affect the dataset. These issues have motivated studies such as the one of Li *et al.*[23] where a Convolutional Neural Network (CNN)-based methodology has been applied to bridges with different crack patterns.

The combination of machine learning techniques with image processing approaches has proven to deliver promising results[25]. In DIP, color images are represented as a matrix of vector-valued pixels formed by the intensity values of the red, green, and blue components of the image[26]. DIP techniques may involve spatial and frequency domain filtering, segmentation (e.g., thresholding or edge-based techniques), and mathematical methods (e.g., morphological operations)[12,27,28]. Each of these methods encompasses widely accepted techniques. Indicatively, spatial domain filtering is applied by employing mean, median, Winer, and Gaussian methods for denoising converted grayscale images[29]. Thresholding approaches rely on the implementation of image binarization algorithms presented in leading-edge works including the Otsu (1979)[30], Niblack (1986)[31], and Sauvola (2000)[32] algorithms. Moreover, among the most commonly used edge detectors for crack detection are the ones of Sobel (1968)[33] and Canny (1986)[34]. Finally, mathematical methods include morphological operations such as erosion, dilation, or closing to remove irrelevant pixels to cracks or fill the gaps to continue the cracking pattern[35]. All of these image-processing aspects are usually combined to achieve a reliable and accurate cracking output[35] thus triggering several researchers to upgrade practices for DIP crack detection.

Despite the popularity gained in image processing and deep learning techniques, their implementation in UAV-collected data is limited to images captured at a very short distance from the structure (e.g.,[18,23,36]). This is mainly attributed to the specifications of image resolution and pixels required to achieve reliable results. Currently, the issue of pixel-level crack detection has been examined by[37]. The authors reviewed deep-learning-based crack image segmentation techniques and they presented the requirements for their applications.

Within the context of a UAV-based SHM program for civil structures such as port concrete infrastructure, UAV flights are typically conducted at higher altitudes than those currently applied for UAV-based crack detection (e.g.,[19,38]). The flight altitude is optimized to capture a detailed overview of the entire structure while obtaining an acceptable number of images for analysis. The set of individual UAV images can be analyzed with photogrammetry applications to generate surface profiles of the 3D structures (i.e., orthophotos) thus providing geospatial information for detected defects (e.g., cracks)[39]. Once geospatial metadata is acquired, GIS tools can be used to examine structural features[19,39]. Despite the positive feedback from current research on combining UAV-based photogrammetry and GIS applications for assessing the structural condition of concrete structures, this synergy has not yet been integrated into DIP practices. Existing image-based methodologies often overlook geospatial information as their main focus is on a limited and predefined number of UAV images.

Considering the above, the present paper bridges two research gaps in automating crack detection in port concrete pavements. The first one is related to taking advantage of UAV geospatial information and mapping cracks on orthophotos illustrating the entire structure. One of the main challenges is to find suitable UAV flight altitudes that do not compromise accuracy. The second issue is the unexplored implication of GIS tools in assisting automation processes for crack detection and propagation monitoring. Within the framework of this research, an insightful approach is presented to work on geospatial metadata (i.e., orthophotos). A structured methodology is proposed and tested on orthophotos obtained from periodic inspections. The contribution of the present work includes the following:

- Retaining the geospatial information throughout the entire process of crack detection in port concrete pavements while processing orthophotos is achieved by importing specific modules and tools in programming and GIS environments.

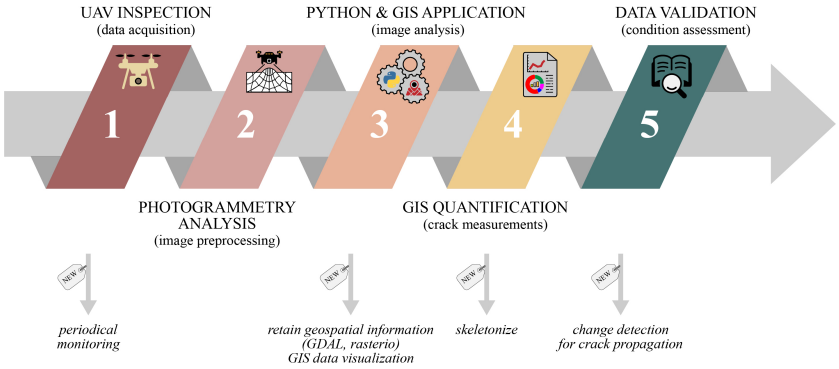

Figure 1. Stages for advanced crack detection in port concrete infrastructure (source: own work).

- The potential of GIS tools in improving crack detection and structural performance assessment is realized. GIS environments offer a range of features that, when combined effectively, enable visualizing, editing, locating, and quantifying cracking results.
- The regular update of the GIS database fed with all comprehensive information on the structural condition of port concrete infrastructure in terms of cracking is encouraged. This enables the identification of variations in crack patterns and propagation issues over the structure's lifespan. Moreover, the causal relationship between crack propagation and forcing factors (e.g., loading conditions) can be examined. Hence, informed decisions regarding maintenance and rehabilitation strategies can be made for effective Life-Cycle Management of the structure.
- The georeferenced output can be combined with structural data related to different port structures and included in GIS databases, thus providing a comprehensive understanding of the vulnerabilities within the entire port system.

2.2 Methodology

The overarching framework for mapping cracks in port concrete infrastructure by combining DIP and GIS modules includes five Stages [Figure 1]. Data acquisition is achieved by employing high-resolution cameras mounted on UAVs following a periodic SHM program (Stage 1). Factors such as the flight altitude, the camera filters, the environmental conditions, etc., affect the quality of the collected imagery. UAV data are processed with photogrammetry analyses to generate geospatial metadata (i.e., orthophotos) (Stage 2). The implementation of Stages 1 and 2 is summarized in Figure 2. Further details regarding the principles and the methods for applying Stages 1 and 2 can be found in the study of[19].

Stages 1 and 2 are crucial for initiating crack detection applications. Once geospatial metadata (i.e., orthophotos) is acquired, Stages 3, 4, and 5 of Figure 1 are applied based on a structured methodology proposed in the present paper [Figure 3]. These Stages include image-based processing techniques and GIS tools. Two open-source environments are employed for the programming and GIS processes: (a) QGIS (version 3.22); and (b) Spyder (version 5.4) for Python language, respectively. QGIS tools are used for visualizing georeferenced metadata and converting raster data (i.e., images) to vector data for mapping and quantifying cracks (Stages 3, 4, and 5). Python language is used for applying image processing algorithms and validation of the proposed methodology (Stages 3 and 5).

The novelty of the proposed methodology is identified in two critical points: (a) working on orthophotos of large surfaces with port concrete pavements and retaining the geospatial information during all steps of image analysis; and (b) integrating GIS tools in automation processes for detecting cracks and monitoring propagation. During the implementation of Stages 3, 4, and 5 working with geospatial data is achieved by integrating the following two libraries into image analysis:

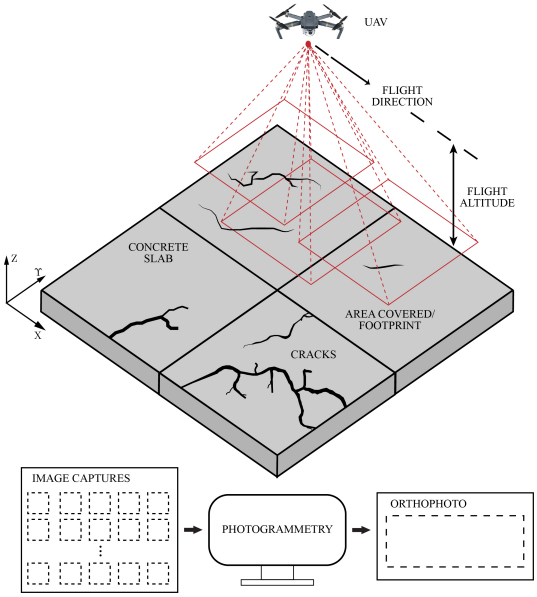

Figure 2. UAV-based data acquisition and photogrammetry applications - Stages 1 and 2 of Figure 1 (source: own work).

- The Geospatial Data Abstraction Library (GDAL) for translating and processing both vector and raster data[40].
- The Rasterio library for reading writing and processing geospatial raster data[41].

The methodology outlined in Figure 3 describes how modules and tools for image processing and GIS applications are interconnected to analyze georeferenced images for crack detection on port concrete pavements. All programming steps of the proposed methodology are summarized in Figure 4. It is noted that the present study does not produce new algorithms and methods for crack detection but rather offers a novel approach for managing orthophotos and leveraging GIS tools. Therefore, existing practices are upgraded with geospatial information analysis. The methodology can be customized to suit specific needs, such as incorporating edge detection algorithms. The primary focus is on preserving the geospatial information throughout the image processing analysis to assess the structural condition of port concrete pavements effectively.

2.2.1 *Study area definition*

Orthophotos typically represent a large part of port infrastructure. To avoid computer crashes and increase the speed of computations, orthophotos are clipped with GIS tools to match the area that will be further examined thus creating a new RGB image. This area is normally defined by considering existing structural conditions (e.g., the presence of cracks that propagate, the occurrence of a sudden event that caused surface cracking, *etc*.), the application of a maintenance scheme, a future upgrade, *etc*.

2.2.2 *Crack digitization*

Crack digitization is essential to verify crack detection results. It is performed in the initial color image of the study area by utilizing GIS tools including changing the layer blending mode, the brightness, the saturation, the contrast, and the Gamma value[19]. The main challenge in this step is to exclude the linear illustrations that are irrelevant to cracks such as marks from dragging equipment or loads.

2.2.3 *Grayscale conversion of the RGB image*

The new georeferenced RGB image is decolorized and converted into a grayscale image with programming modules [Figure 5]. This modification is important to eliminate color information that complicates computational requirements for crack detection[42]. The algorithm used for the conversion is described in Equa-

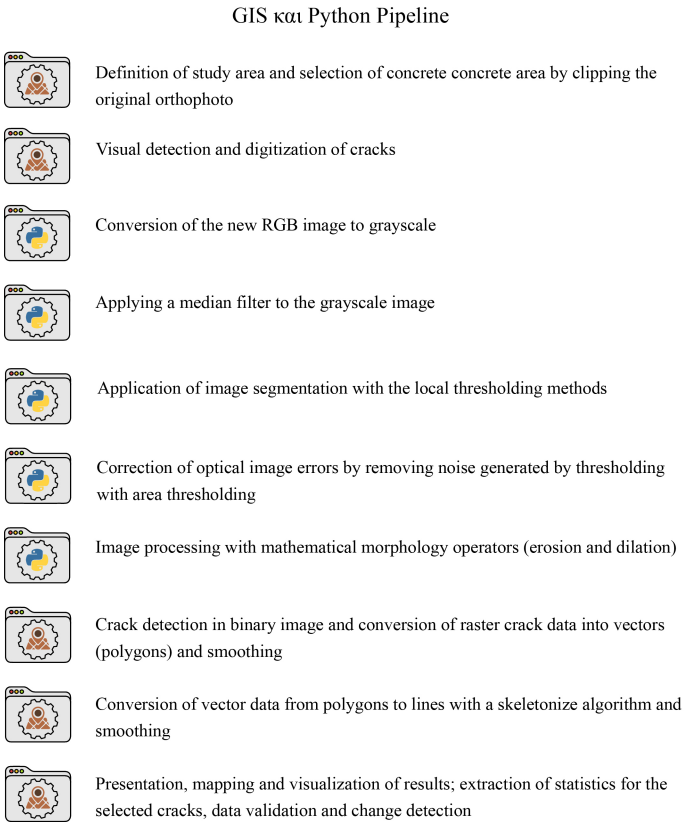

Figure 3. Methodology for mapping cracking in port concrete infrastructure by working on geospatial metadata - Stages 3, 4, and 5 of Figure 1 (source: own work).

tion (1)[43].

$$Y = 0.299 * R + 0.587 * G + 0.114 * B \quad (1)$$

where R, G, and B are a linear representation of the Red, Green, and Blue channels of a pixel, respectively.

2.2.4 *Median filtering*

A common task in DIP is noise removal. Median filtering is applied to the georeferenced grayscale image to reduce the degree of intensity variation between two pixels while avoiding non-realistic values[44]. To apply the median filter, a sliding window (i.e., kernel) is placed at a specific pixel of the image and all pixel values included in this window are placed in ascending order to compute the median value assigned to the pixel[43] [Figure 6].

2.2.5 *Image segmentation with thresholding*

Thresholding is a common segmentation approach for partitioning images into regions based on different ranges of pixel values[26,45]. To achieve this, intensity histograms are built [Figure 7]. The thresholding value t can be either constant for the entire image (global thresholding) or changing over the image (local thresholding). Indicatively, local thresholding with Otsu's algorithm[30] defines different threshold values with block-based or sliding-based windows depending on the lighting conditions and the different features of the image. This algorithm searches for a threshold t that maximizes the variance between the foreground (cracking) and background (no-cracking) groups or minimizes the variance within the group. All pixel values below the

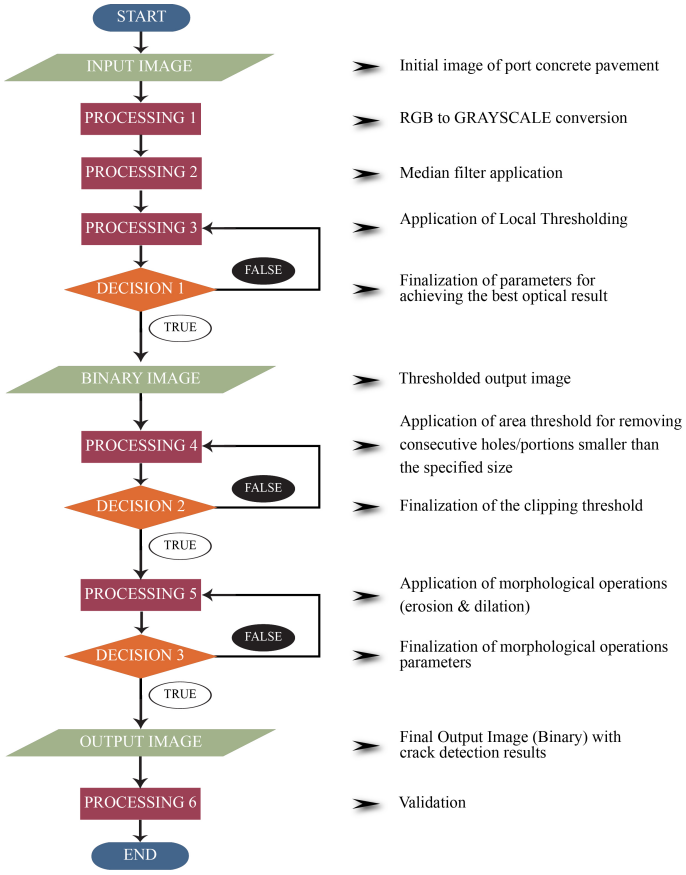

Figure 4. Flow chat of programming-based image processing for crack detection in port concrete pavements (source: own work).

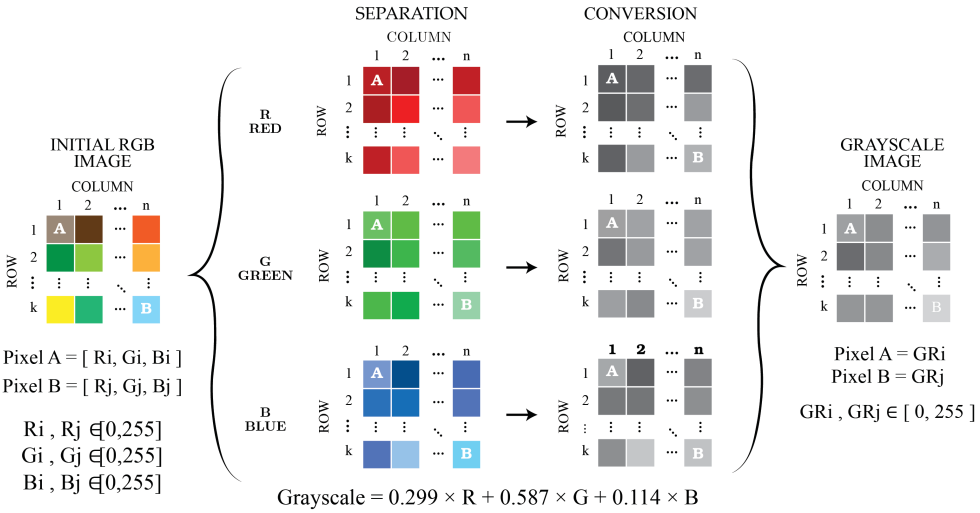

Figure 5. Procedure for converting an RGB image to a grayscale image (source: own work).

threshold are set to zero, while those above the threshold are set to one (image binarization). The variance within the groups v_{within} is given by

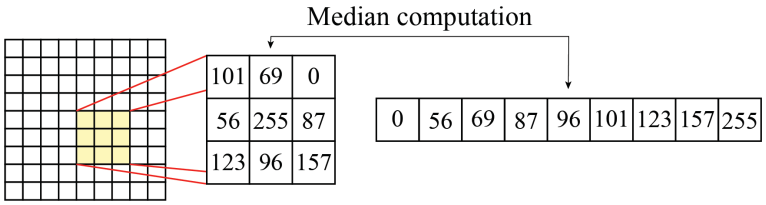

Figure 6. Example of median filtering (source: own work).

$$v_{within} = P_b(t) * v_b + P_f(t) * v_f \tag{2}$$

while the variance in between the groups $v_{\text{inbetween}}$ is given by

$$v_{inbetween} = v - v_{within} = P_b * P_f(m_b - m_f)^2 \tag{3}$$

where $P_b(t) = \sum_{i=0}^{t} p_i$ is the probability of the background pixels, $P_f(t) = \sum_{i=0}^{t} p_i$ is the probability of the foreground pixels, p_i are the probabilities, v_b is the variance of the background, v_f is the variance of the foreground, v is the variance of the entire image, $m_b = \sum_{i=0}^{t} i \cdot p_i$ is the average intensity of the background, and $m_f = \sum_{i=0}^{t} i \cdot p_i$ is the average intensity of the foreground.

2.2.6 Noise removal in the binary image

The presence of shadows, tire marks, and other image noises may be translated as cracking during image thresholding. To address this problem and avoid misinterpretation of results, noise removal is repeated by measuring the properties of the irrelevant-to-cracks black areas in the binary image and isolating them with a new threshold. Label tagging is conducted based on the calculated area represented by the number of irrelevant white pixels.

2.2.7 Morphological operations

Two morphological operations are used in the current research: dilation and erosion [43]. With dilation, small holes in the cracking pattern are filled. A rectangular structural element is placed over every pixel of the binary image and its pixel values are compared with the ones of the image [Figure 8]. Initially, the dilation process identifies the boundary pixels of the crack. Thereafter, it grows the boundary by a specified number of pixels. Multiple iterations are usually required to achieve accuracy in crack detection. On the other hand, erosion is used to remove pixels from the binary image, once dilation is completed. Similar to dilation, erosion places a rectangular structural element over every pixel of the image. However, it shrinks the boundary of the crack by a specified number of pixels.

2.2.8 Vectorization of the detected cracks

The key point of the implementation of all previous steps of the proposed methodology is retaining the geospatial information of the image. Hence, crack detection in port concrete infrastructure is expanded beyond image-based modules in programming and advanced by employing GIS tools. GIS-based vectorization of the binary image enables converting raster data (an array of pixels) to polygons [46] thus identifying crack features. Once achieved, smoothing processing is also applied to enhance the visual display and the continuity of the vectorized cracking data by reducing sharp angles and irregularities. The output of the vectorization step provides geospatial information about the width of the detected cracks [Figure 9].

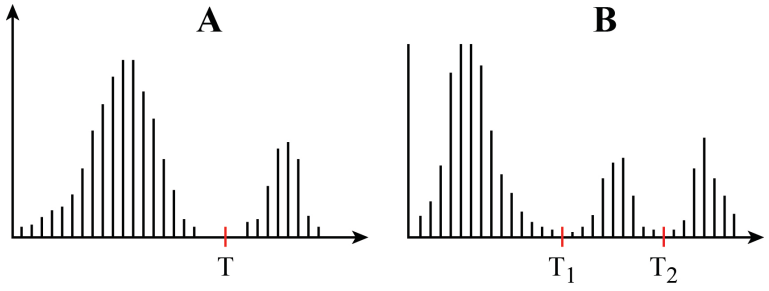

Figure 7. Indicative example of a histogram. A: Use of one threshold and B: use of multiple thresholds (source: own work).

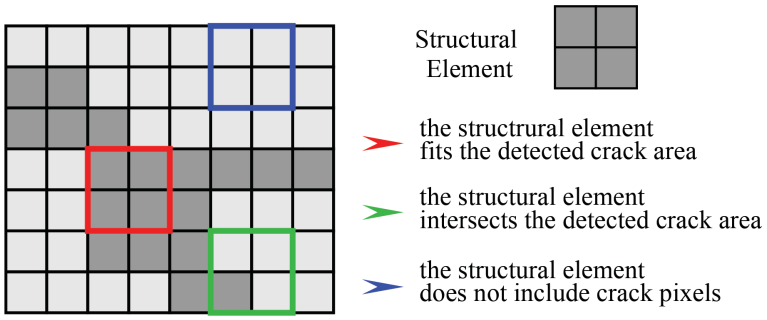

Figure 8. The sliding structural element during morphological operations (source: own work).

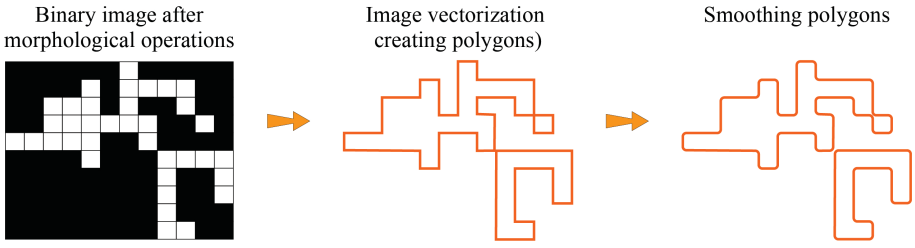

Figure 9. Vectorization of raster data of the binary image once morphological operations are completed (source: own work).

2.2.9 *Skeletonization of vectorized crack data*

Except for the width, additional information regarding the crack length is usually required when inspecting and assessing the condition of concrete structures. GIS-based skeletonization follows vectorization to generate linear illustrations of the detected cracks. The skeletonization algorithm processes the polygon geometry to recognize the pattern of the detected cracks[47]. Similar to the vectorized data, smoothing processing is also applied.

2.2.10 *Crack data validation and change detection*

The validation of the crack detection results is conducted by forming a confusion matrix, i.e., an n × n array that includes information for the automatically detected (predicted) cracks and the manually detected (digitized) ones[48]. The comparison requires raster data. To ensure comparable datasets, digitized cracks are converted to raster data (rasterization). During this process, it is important to ensure that the pixel size of the digitized cracks is equal to the one of the detected cracks. The confusion matrix is used to calculate the sensitivity, specificity, false-positive rate, false-negative rate, positive predictive value, negative predictive value, accuracy, and F1 score[49] [Figure 10]:

- The "Sensitivity" or "Recall" is a measure that indicates to what extent the detection model correctly iden-

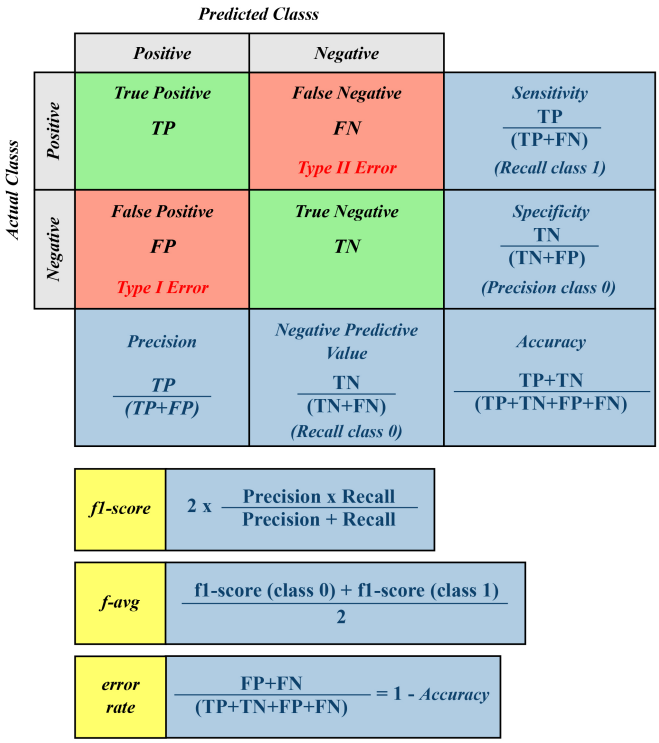

Figure 10. Confusion matrix (Source: Own work based on the studies of Obi [48] and Tharwat [49].

tifies the True positive pixels.

- The "Specificity" or "Precision" is a measure for determining the percentage of positive identifications that are correct.
- The "Accuracy" is a measure that indicates the number of times the detection model correctly identified the data class (i.e., 0 or 1) across the entire dataset.
- The F1-score links "Sensitivity" to "Specificity" by calculating their harmonic mean.

3 RESULTS

Within the context of the current research, the selected study area includes a concrete part of the domestic ferry terminal pavement of a Greek port, namely Lavrio port. Lavrio port is located at the southeastern tip of Attica (37°42′44″ N, 24°3′25″ E) [Figure 11] and is listed as a port of national importance (https://oll.gr/en/). The concrete pavement of the domestic ferry terminal is continuously exposed to loading and environmental conditions, thus threatening its structural integrity. During four UAV-based ISIs conducted on 2020-02-10 (ISI-1), 2020-09-04 (ISI-2), 2021-02-10 (ISI-3), and 2021-07-09 (ISI-4), it was observed that the pavement in the defined concrete area (enclosed within a black outlined rectangle in Figure 11 was severely and continuously cracked. The ISIs were conducted with the DJI MAVIC 2 pro UAV while UAV collected data was analyzed with Agisoft software (version 1.6.4) to generate the orthophotos.

The mean flight altitude of each UAV inspection was 48, 56, 76, and 56 m while the ground resolution was 1.06, 1.21, 1.66, and 1.17 cm/pixel for ISI-1, ISI-2, ISI-3, and ISI-4, respectively. The varying altitudes were applied to investigate the impact of these different flight characteristics on acquiring and analyzing SHM data for port concrete structures. Further details regarding data collection and analysis (Stages 1 and 2 of Figure 1) can be accessed through relevant work [19]. The flight altitude and the ground resolution of ISI-3, as well as the presence of a large shadow within the study area [Figure 12], resulted in the exclusion of the georeferenced

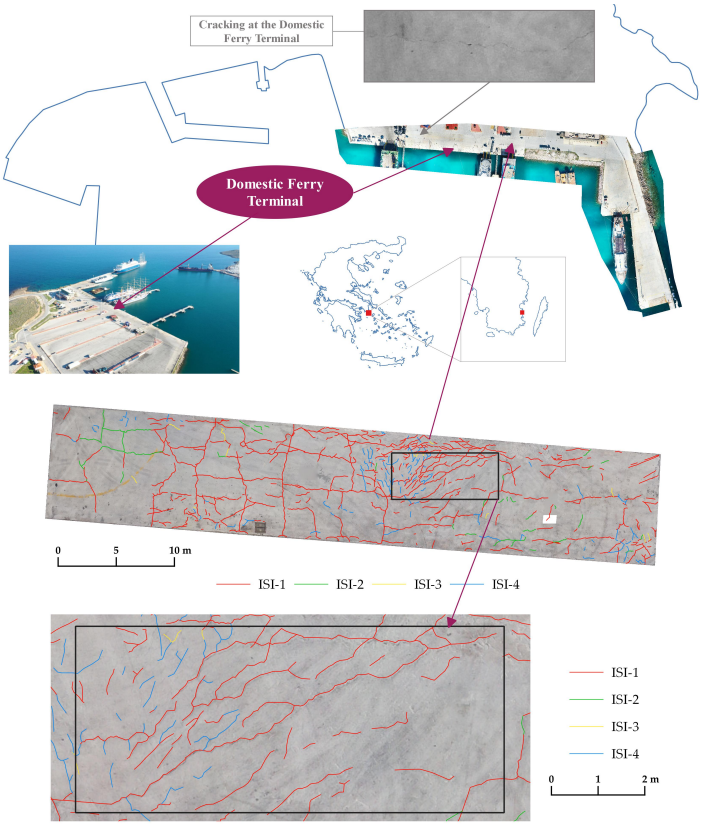

Figure 11. Definition of the study area in Lavrio port, Attica, Greece enclosed within the black outlined rectangle. Red-colored crack lines are digitized based on ISI-1. Green-colored crack lines are the new and/or propagated digitized cracks based on ISI-2 for the time interval between ISI-1 and ISI-2. Yellow-colored crack lines are the new and/or propagated digitized cracks based on ISI-3 for the time interval between ISI-2 and ISI-3. Light blue-colored crack lines are the new and/or propagated digitized cracks based on ISI-4 for the time interval between ISI-3 and ISI-4. The crack digitization process involved using GIS tools to visually detect cracks by working on the orthophotos of each ISI. (source: own work).

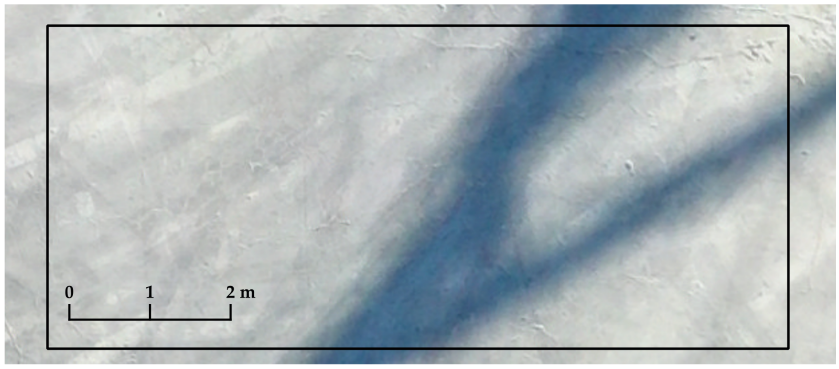

Figure 12. Georeferenced image of the study area based on ISI-3.

image of ISI-3 from the crack detection process.

Once the study area was defined, the georeferenced image clipped from the orthophotos was converted to a grayscale image based on the procedure described in Section 2. A median filter with a 3×3 kernel was implemented in the grayscale image to eliminate noise and local thresholding was applied to binarize the

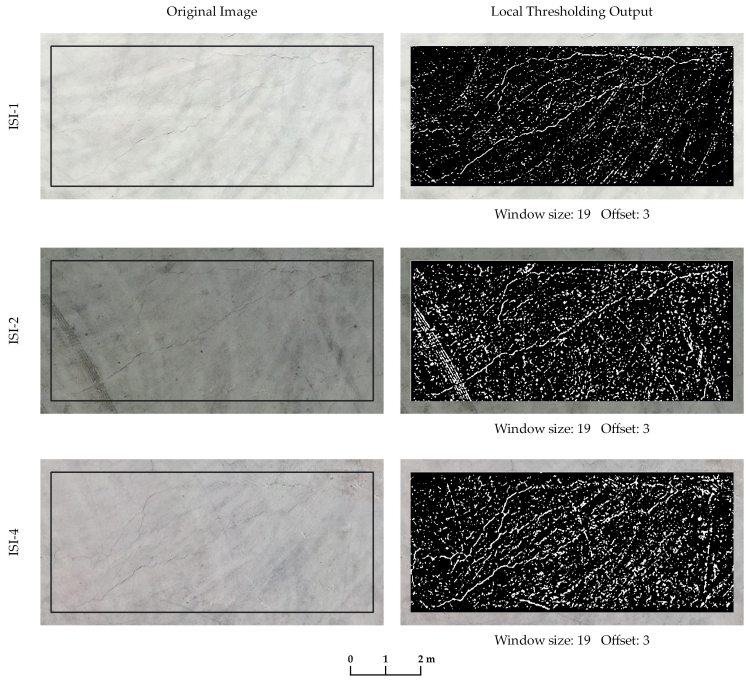

Figure 13. Illustration of the severely cracked area of the examined concrete pavement of Lavrio port once local thresholding was applied for each ISI.

image. Figure 13 shows the image results after the segmentation and the values of the window size and the offset required for the application of the local thresholding algorithm. By examining Figure 13 it is observed that the noise includes not only linear elements/groups of pixels but also circular or ellipsoid shapes. Following similar practices for removing noise after segmentation [30], denoising was applied with a threshold of 15, 25, and 28 pixels for each binary image, respectively [Figure 14].

Although noise removal resulted in improving crack detection, random white pixels remain present. During the digitalization of cracks [Figure 11], it was observed that cracks thinner than 15 mm approximately, detected while conducting visual inspections at Lavrio port, were difficult to identify in the GIS-based visualization. Based on the study of Yang *et al*., the ability to detect thin cracks depends on the image-capturing distance of the camera, the light conditions, the exposure time, and the pixel size [50]. Cracks thinner than one pixel cannot be easily measured. Hence, for the present research, white pixels beyond the area of the main cracking illustrated in Figure 15 were excluded as shown in Figure 16. The cracks shown in Figure 15 were manually digitized using GIS tools, while the cracks in Figure 16 are the result of applying area thresholding.

By examining Figure 16, it was observed that the continuity of the cracks formed by adjacent pixels was interrupted in some areas, while several white irrelevant pixels were present. Based on the described methodology in Section 2, the dilation process was first applied to achieve the optimal filling with white pixels without imperiling over increasing crack width [Figure 17]. A 3×3 structural element was used and the process was repeated twice. Once dilation was completed, erosion was implemented twice with a 3×3 structural element to remove false pixels that existed previously or had occurred during the previous morphological operation [Figure 18]. A more detailed example of the significance of the morphological operations is shown in Figure 19. A crack pattern identified in the initial georeferenced image was effectively detected after the implementation of all steps of the proposed methodology up to the level of completing erosion even though some gaps still exist. Furthermore, although a significant part of the noise was removed, some irrelevant white pixels are still present.

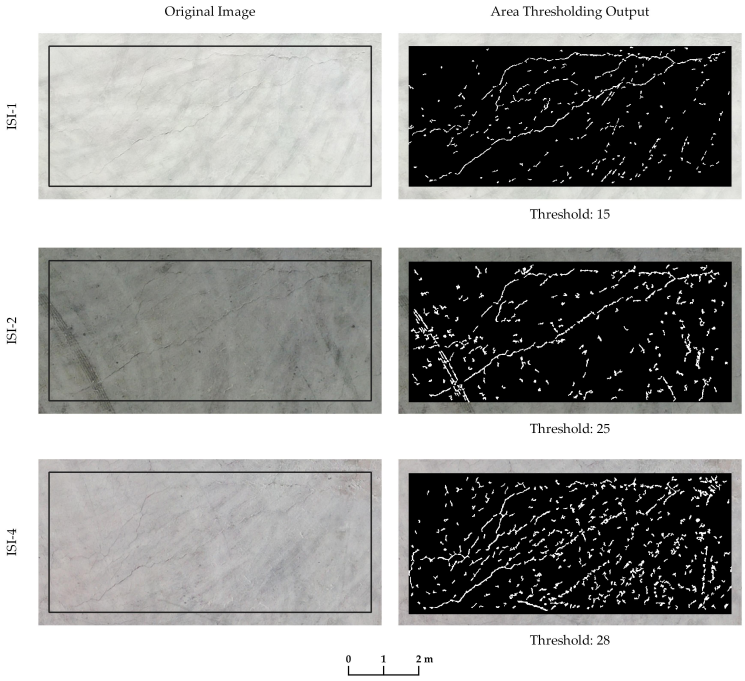

Figure 14. Illustration of the severely cracked area of the examined concrete pavement of Lavrio port once area thresholding was applied to the binary images of each ISI.

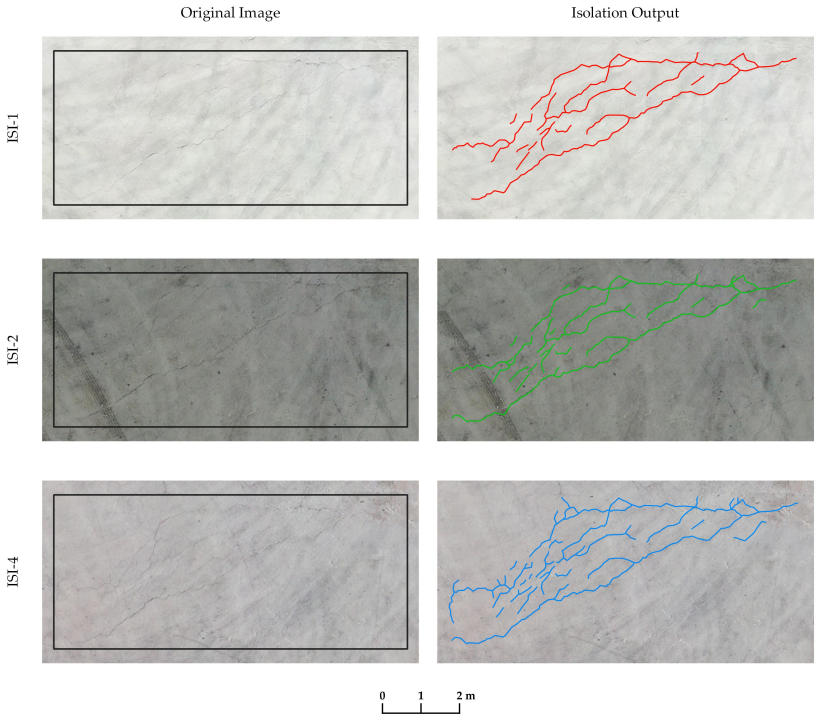

Figure 15. Isolation of the cracked area showing the digitized crack output acquired through visual examination of the orthophotos.

The GIS-based visualized output of crack detection processing in the study area is shown in Figure 20, while the rasterized output generated by the application of the morphological operations was vectorized and the

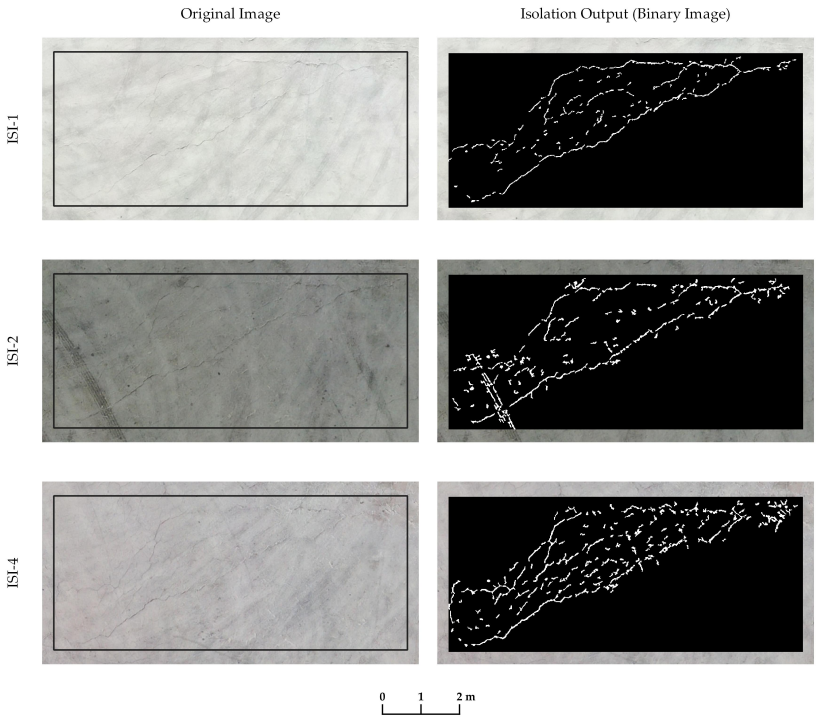

Figure 16. Isolation of the cracked area in the binary image of Figure 14.

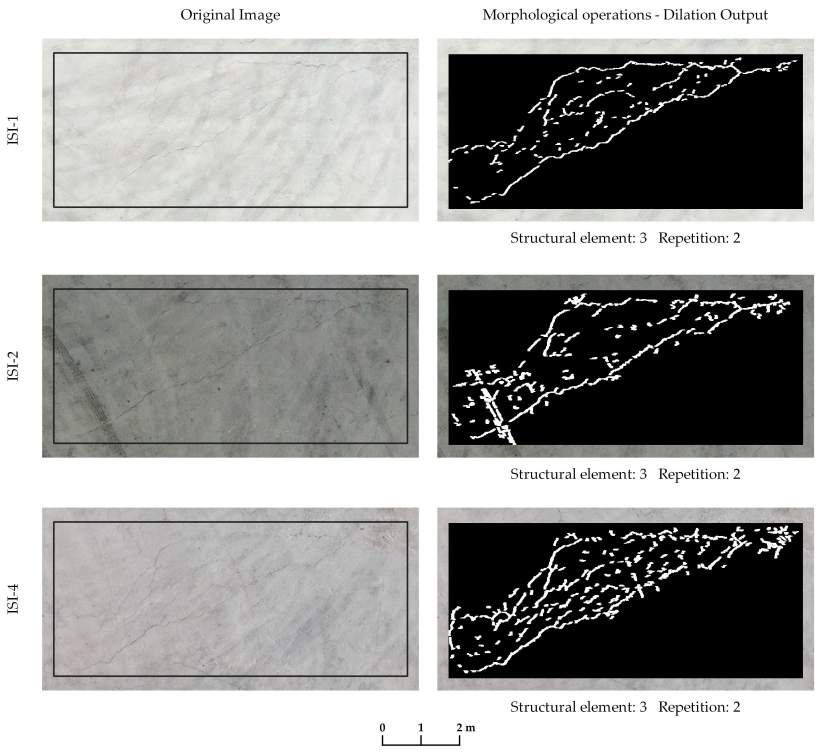

Figure 17. Morphological operations - Dilation output for the considered cracked area.

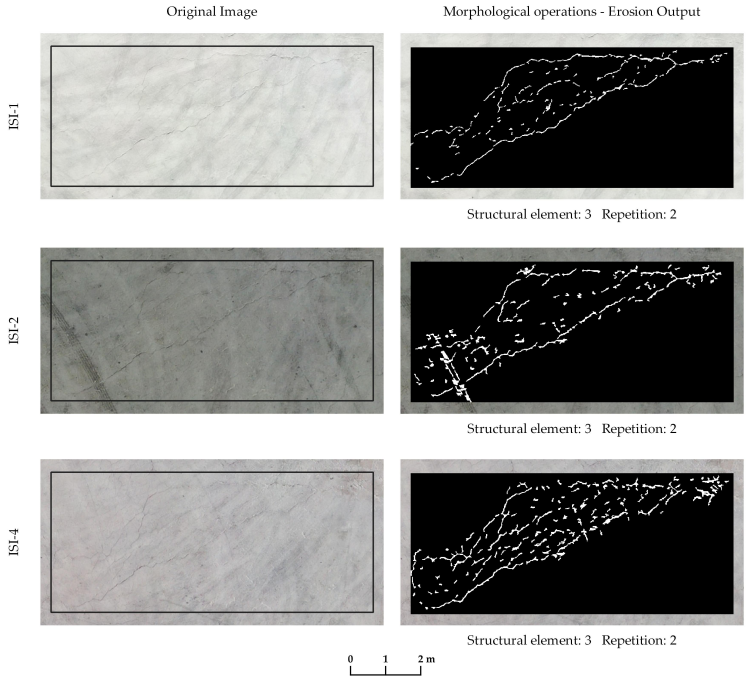

Figure 18. Morphological operations - Erosion output for the considered cracked area.

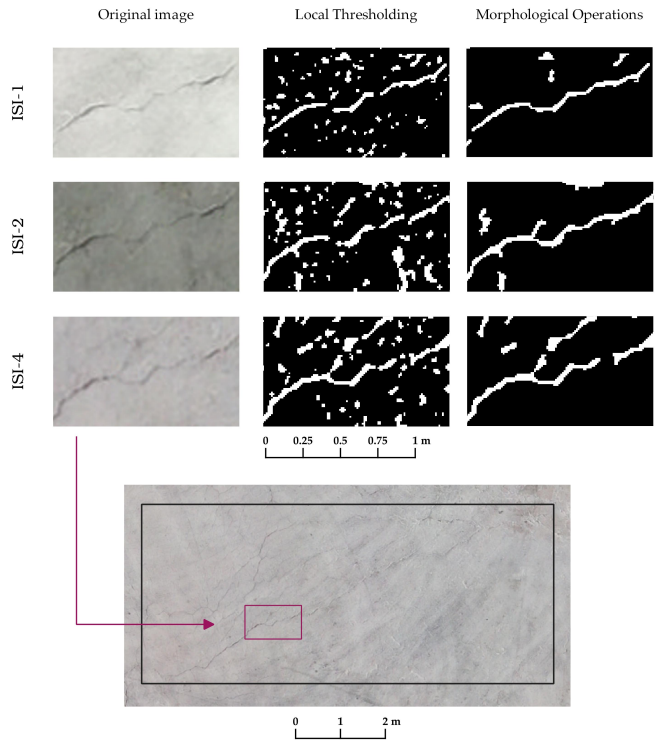

Figure 19. A detailed illustration of the detection of a crack pattern after morphological operations are completed.

final output of the skeletonization is included in Figure 21. Indicatively, the separate steps of subsequently converting raster data to polygons and lines are reflected in Figure 22 for the example of Figure 19. Moreover,

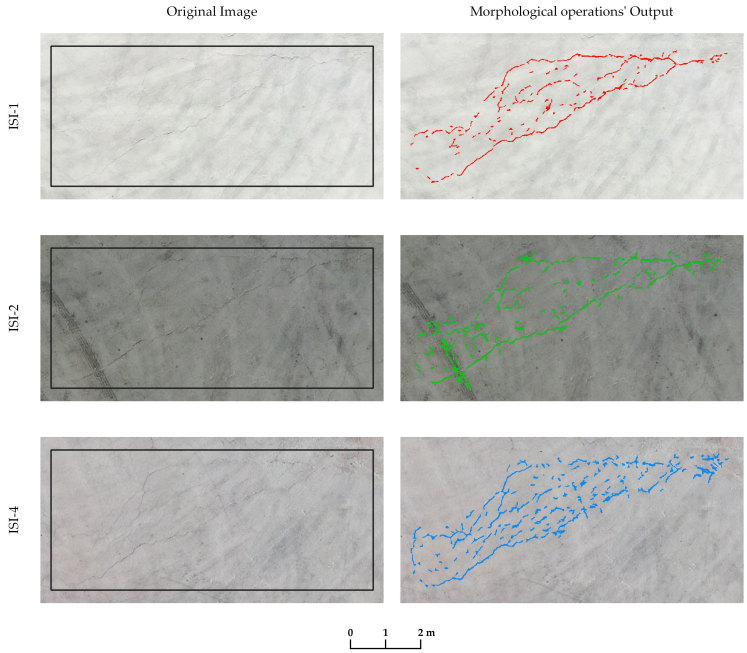

Figure 20. The GIS-based visualized output of crack detection processing after morphological operations are completed. Cracks are depicted as polygons.

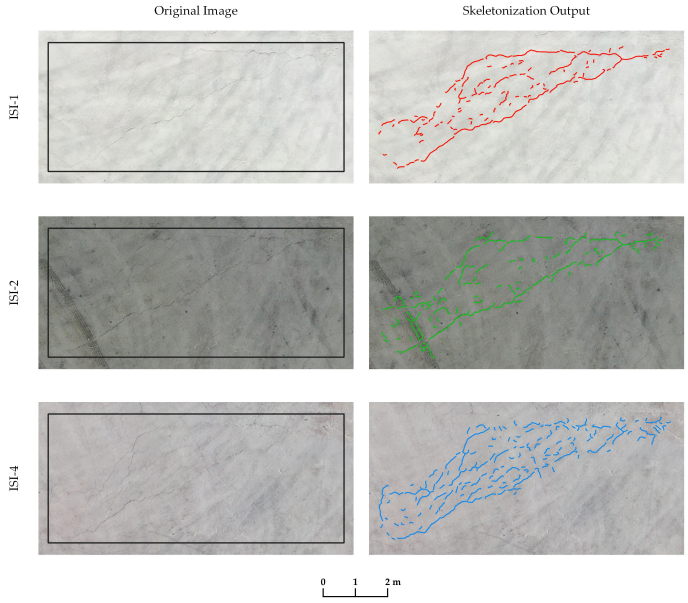

Figure 21. Final output of crack detection based on the proposed methodology. Cracks are depicted as lines with the skeletonization algorithm.

Figure 23 includes a comparison between digitized (i.e., manually detected) and vectorized (i.e., automatically detected) cracks for the same area as in Figure 19.

Based on Figure 23, it is noticed that the digitized primary crack of 28 mm width of ISI-1 is efficiently detected. Both crack features (i.e., width and length) and dark appearance in the original image were the main factors

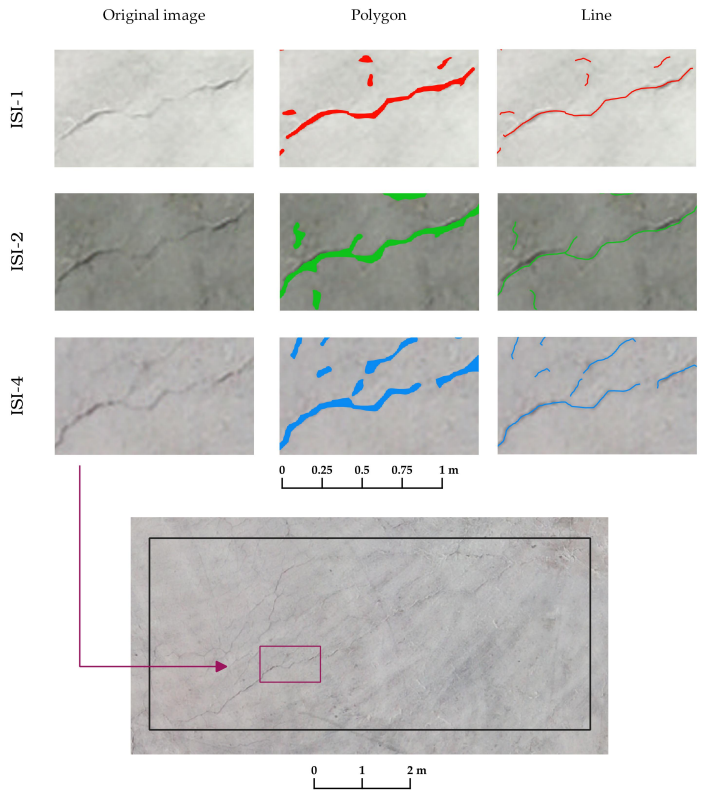

Figure 22. Vectorization of the rasterized output of the example illustrated in Figure 19.

that facilitated crack detection. However, for the remaining cracks thinner than 15 mm crack detection failed. Moreover, three additional lines of 10-15 cm length appeared after image processing mainly due to color tone differentiation from the adjacent pixels. Similar to ISI-1, the primary crack of ISI-2 was also detected along with some false lines. An additional vertical crack was digitized and partially detected. This crack seems to propagate during the time intervals of the ISIs as shown in the results of digitization and detection for ISI-4. Crack detection for ISI-4 resulted in identifying the primary crack and its diagonal propagation, while similar to the inspections ISI-1 and ISI-2 false lines were also present. Considering the above, it is highly interesting that the proposed GIS-based methodology enables detecting structural variations during port concrete pavements' lifetime in terms of crack propagation.

The above observations were validated by building the confusion matrix described in Section 2. Before proceeding with validation, the digitized (i.e., manually detected) crack lines were converted to polygons to measure the crack width with GIS rasterization tools, as indicatively shown in Figure 24. The characteristics of the digitized cracks are included in Table 1. Figure 25 shows a comparative illustration of the digitized and detected width data for the example of Figure 19. It is obvious that for the specific illustration, the crack width is increasing between inspections. This observation indicates a continuous progression of the damage in the concrete pavement, highlighting the need for timely maintenance interventions.

To validate the results for the entire study area, the performance metrics were calculated based on the developed confusion matrix illustrated in Figure 10 [Table 2 and Table 3]. More specifically:

- The high "Sensitivity" percentages of ISI-1 and ISI-4 show that a large amount of the digitized cracks was successfully detected contrary to the digitized cracks of ISI-2 that were partially detected.
- The significantly high "Specificity" percentage of all ISIs indicates the high accuracy in classifying the non-

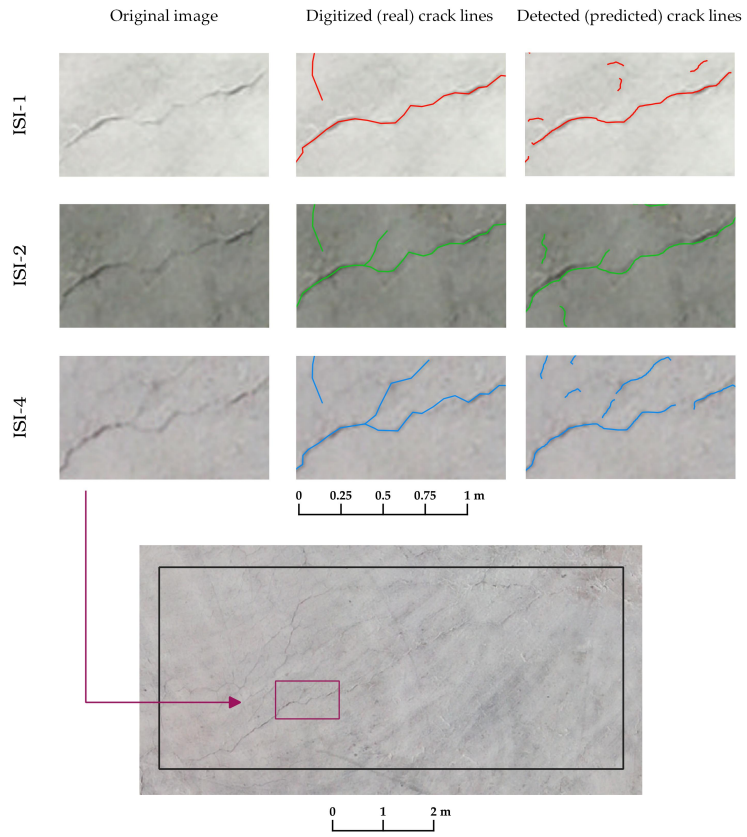

Figure 23. An indicative comparative illustration between digitized (i.e., manually detected) and vectorized (i.e., automatically detected) cracks for the example of Figure 19.

cracked areas.

- The average "Precision" percentage of the order of 68% of all ISIs demonstrates that within the total amount of cracks detected by applying the methodology, approximately 32% of them were false.
- The significantly high "Negative Predictive Value" of all ISIs indicates that the probability that a case is truly negative (non-cracked area) among the cases predicted as negative is very high.
- The high "Accuracy" percentage between 90% and 100% shows that the classification of non-cracked and cracked areas is mainly correct considering the entire sample.
- The F1-score for the class 0 is between 95% and 100% thus demonstrating that the "Sensitivity" and "Specificity" do not deviate from each other and the majority of predictions for the non-cracked areas are correct.
- The F1-score for class 1 is between 74% and 76% for ISI-1 and IS-4 thus demonstrating that the "Sensitivity" and "Specificity" deviate slightly from each other and that 3/4 of predictions for the cracked areas are correct. On the other hand, the F1-score for ISI-2 is reduced up to approximately 57%. Considering this, it seems that the detection model can be improved to avoid F1-scores for class 1 below 70%
- The average F1-score is above 70% thus indicating a total satisfactory balance between "Sensitivity" and "Specificity". In other words, the detection model is performing well.
- The error rate for ISI-1 and ISI-4 ranges between 2% and 3% thus verifying the high accuracy of the model. The increased error rate of ISI-2 is linked to the detection model's liability to falsely detect cracking in some cases where noise is significantly high. This is attributed to the presence of tire marks [Figure 20] which causes the detection model to classify the dark marks as cracks.

Analysis of Table 2 and Table 3 revealed that even though ISI-2 and ISI-4 had the same UAV flight altitude, ISI-4 outperformed ISI-2 in terms of performance metrics and F-score values. The presence of intense noise

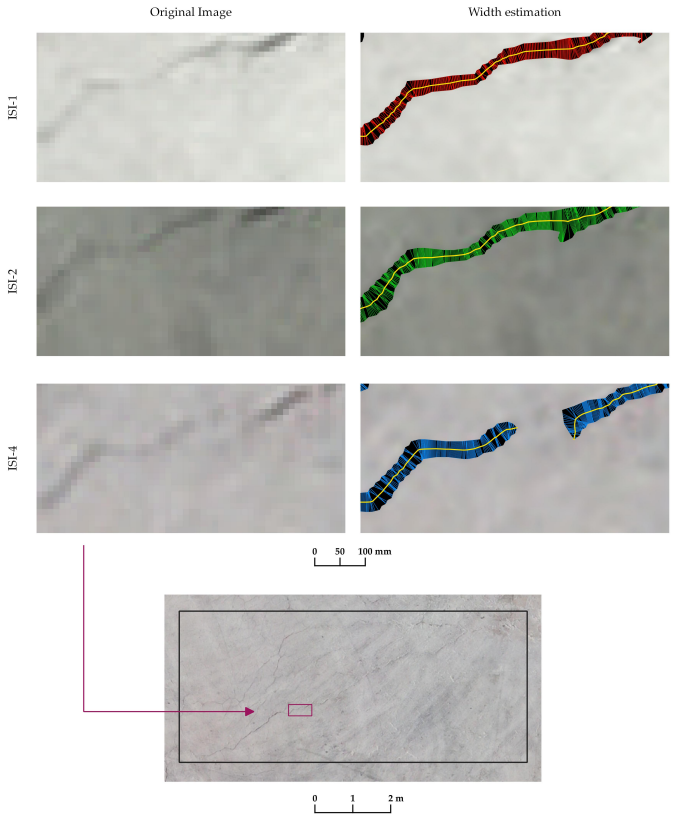

Figure 24. Example of width estimation of digitized crack lines with GIS rasterization tools.

Table 1. GIS-based measurements of the digitized cracks

ISI-i	Total length (m)	Minimum width (mm)	Maximum width (mm)	Average width (mm)
ISI-1	23.65	14.4	82.0	28.5
ISI-2	23.15	13.8	96.0	37.5
ISI-4	27.88	15.2	89.0	36.5

Table 2. Performance metrics for validating crack detection results for the example of Figure 19

ISI-i	Sensitivity	Specificity	Precision	Negative predictive value	Accuracy
	(Recall class 1)	(Precision class 0)	(Precision class 1)	(Recall class 0)	
ISI-1	84.29%	98.12%	66.22%	99.38%	97.62%
ISI-2	56.09%	96.90%	60.81%	95.39%	92.91%
ISI-4	73.53%	98.65%	79.35%	98.17%	97.02%

from the tire marks in ISI-2 had a negative impact on result precision. However, despite this noise, the performance values were still relatively high, indicating that the proposed methodology shows promise even in the presence of noise. Additionally, a variation of 10 m in the UAV flight altitude did not seem to adversely affect the performance of the proposed methodology. Crack detection using data collected from flights at altitudes ranging from 48 to 56 m exhibits high precision. Hence, the methodology maintains its robustness across this range of altitudes.

By combining the GIS-based quantified results for the digitized cracks included in Table 1 and the F-scores of

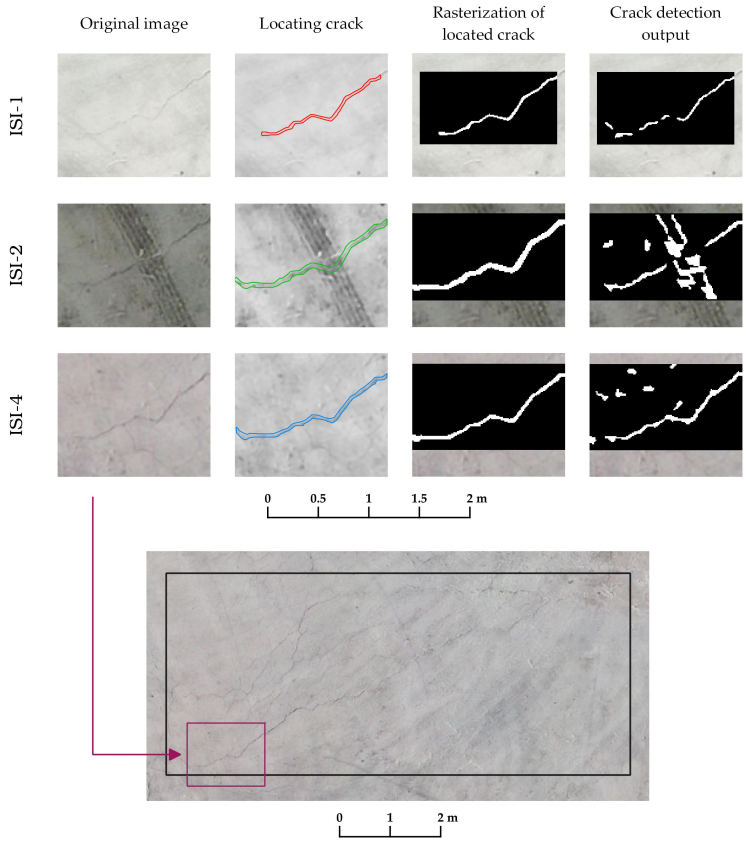

Figure 25. A comparative illustration of the digitized and automatically detected width data for the example of Figure 19.

Table 3. F-score values for validating crack detection results for the example of Figure 19

ISI-i	F1-score - non-crack area (class 0)	F1-score - crack area (class 1)	F1-score Avg	Error rate
ISI-1	98.75%	74.04%	86.39%	2.38%
ISI-2	96.13%	57.44%	76.78%	7.09%
ISI-4	98.41%	76.12%	87.26%	2.98%

Table 3, the measurements of the truly detected cracks can be derived [Table 4]. During the time period from ISI-1 to ISI-4, there was a noticeable increase in the cracked area, which expanded by 3.71 m in length. This time-induced variation can be visually represented with GIS tools as indicatively shown in Figure 25. Therefore, it can be viewed that distressed areas and the extent of damage are identified through GIS-based mapping and assessment by comparing crack detection results from each ISI. In this context, geospatial metadata that changes over time, such as crack propagation, can be efficiently monitored and analyzed using the proposed GIS-based crack detection methodology. The results of ISI-2 were not considered for change detection due to the lower F1-score for class 1.

4 DISCUSSION

Automation in damage detection with structural monitoring data is currently one of the most prominent areas of research in various industry fields (e.g., manufacturing systems[51,52]). Regarding concrete civil infrastructure working on automatically detecting cracks is a growing trend that has occupied several researchers (e.g.,[23,24,36,50]). Their main focus was on advancing current methodologies and improving efficiency in de-

Table 4. Measurements of the truly detected cracks.

ISI-i	Total length (m)	Maximum width (mm)
ISI-1	17.51	60.71
ISI-2	13.30	55.14
ISI-4	21.22	67.75

tecting actual cracks with either image processing or machine learning approaches. The impact of such crack detection approaches can be amplified by the competitive advantages of GIS tools. A GIS-based structural condition assessment of port concrete pavements enables geospatially visualizing cracks, straightforwardly measuring crack features, storing geospatial crack data, and creating databases for gaining a deep insight into the structure's vulnerabilities (e.g., causes of crack propagation)[19]. Hence, the proposed methodology combines image processing programming modules with GIS applications to support SHM of port concrete pavements.

One of the main issues encountered during the entire process was the impact of the UAV flight altitude. Crack detection for the ISIs with the lower flight altitudes (i.e., ISI-1 with 48 m, and ISI-2 and ISI-4 with 56 m) was effective due to the smaller pixel size of the generated orthophotos. Therefore , the GIS-based crack visualization was conducted with more pixels. Except for the UAV flight altitude, the presence of intense noise such as large shadows from vessels or tire marks affected the results. The orthophoto of ISI-3 was excluded from the analysis from the beginning since the large shadowed area was represented with a dark color tone that can be misinterpreted as a cracked area. In contrast to ISI-3, the orthophoto of ISI-2 was included in the crack detection analysis to assess how tire marks on the concrete pavement surface impacted the effectiveness of the proposed methodology. By removing the noise with thresholding and labeling it seemed that the negative effect of the tire marks was limited.

Furthermore, the specific research was based on routine ISIs the main function of which is to gather information for planning future maintenance actions[7]. The inspections dictated the course and the priority for maintaining the herein-examined concrete slab due to the high-density cracking. The latter is mainly attributed to the large dimensions of the slab (i.e., the absence of construction joints within a large part of the concrete surface) thus allowing for the forming of significant cracks due to movements (e.g., shrinkage, thermal contraction, *etc*.). This fact was aggravated by the absence of repair measures. During the routine inspections, UAV flight altitudes were selected so that not only the entire concrete pavement of the mooring facilities but also other structures such as rubble mound structures were depicted by optimizing inspection and computation time[19]. However, flight altitude can be reduced for targeted inspections of the specific concrete slab to further quantify detected deterioration and determine its structural significance[7].

Although the present paper focuses on port concrete pavements, the application of the GIS-based proposed methodology can be valuable for other similar structural systems such as airports with concrete aprons. Factors including tire marks, building or vehicle shadows, passengers' moving, and others are common challenges encountered in both port and airport systems. For a successful SHM program of these systems, the updating of GIS databases with cracking information is crucial.

Finally, it is noted that the methodology used in this research relies on parameter selection based on common practices that were most suitable for the specific case study. A trial and error process is required when applying the methodology for the first time. However, once the parameters are finalized, the methodology can be easily repeated. Based on the overall investigation, the following aspects should be considered for the iterative process of trial and error to maximize accuracy:

- The kernel size in the median filtering should preserve details and edges while controlling noise reduction. Using a smaller kernel (e.g., 3×3) can retain fine details, enhancing the accuracy. Employing a larger kernel

may smooth out or blur fine cracks, potentially causing false negatives that lower accuracy.

- The window size in the local thresholding determines the local area for thresholding. A smaller window size (e.g., 19 × 19) increases sensitivity to local intensity variations, aiding in the detection of fine cracks, thus improving accuracy. A larger window may overlook fine cracks, leading to false negatives and decreasing accuracy.
- The offset in the local thresholding affects the inclusivity or exclusivity of cracks. A positive offset (e.g., 3) increases exclusivity, thus reducing false positives and improving accuracy. On the contrary, negative offset increases inclusivity, potentially mistaking noise for cracks and decreasing accuracy.
- Area thresholding refines the binary output of crack detection by eliminating irrelevant white pixels. During the analysis, it was observed that the optimal area threshold varied for each image of the ISIs due to the presence of noise. A lower area threshold was found to be appropriate for ISI-1 since it preserved finer cracks, whereas, for ISI-2 and ISI-4, the area threshold was increased to improve accuracy by filtering out irrelevant pixels.
- The structural element in morphological operations affects the number of false positives and negatives. A smaller structural element (e.g., 3 × 3) can help preserve fine cracks and increase accuracy. A larger structural element may distort or merge cracks resulting in false positives that can compromise accuracy.
- Repetitions in morphological operations are important to refine cracks. A limited number of repetitions is preferred over excessive repetitions since the latter may thicken, merge or remove cracks leading to false positives or false negatives that reduce accuracy.

5 CONCLUSIONS

The overall investigation indicated the significance of expanding crack detection approaches beyond mathematical computations. Interrelating cracking data with structural issues of port concrete pavements is achieved by retaining the geospatial information throughout the process to support GIS-based structural condition assessment applications. By building a GIS database, it was concluded that despite the small time interval between the ISIs (approximately every half a year), crack propagation was a continuous issue. This ongoing process imperils the structural integrity of the examined concrete slab, highlighting the importance of planning inspection schemes for in-service port concrete pavements.

One of the main challenges during the analysis was the presence of various noises in orthophotos, such as surface scratches or tire marks, unlike images focusing on limited cracked parts of a structure. The implementation of the combined methodology showed that high reliability and accuracy (average 95%) can be achieved while preserving all geospatial information. This finding is significant as it encourages the use of orthophotos for analyzing port concrete pavements without compromising accuracy. Additionally, once the approach is applied for the first time to a specific port structure and the arrangement of the steps is determined, processing data and returning results quickly enhance the real-time performance of the methodology.

Although the proposed methodology was applied to cracks wider than 15 mm, it was concluded that once all steps were completed it was more effective for detecting cracks wider than 20 mm. If required, UAV flight altitude can be reduced to detect thinner cracks. For this task, it is essential to investigate the balance between inspection and computation time, while considering a potential entanglement with port operations. Therefore, further research may include sensitivity analysis to define the optimal UAV flight altitude based on the surrounding height conditions and restrictions, the accuracy of the outcome, and the collected amount of data.

DECLARATIONS

Authors' contributions

Contributed to conceptualization, methodology, software, validation, analysis, investigation, data collection, draft preparation, manuscript editing, and visualization: Tsaimou CN
Contributed to methodology, software, analysis, and manuscript editing: Kagkelis G
Contributed to field data collection and validation: Sartampakos P
Contributed to methodology, software, and validation: Karantzalos K
Contributed to conceptualization, methodology, analysis, investigation, data collection, validation, manuscript editing, review, supervision, project administration, and funding acquisition: Tsoukala VK

Availability of data and materials

Not applicable.

Financial support and sponsorship

The first author was supported for this research by the Special Account for Research Funding of the National Technical University of Athens, Greece (Scholarship grant number 65/219100).

Conflicts of interest

Sartampakos P is from NIREAS Engineering, which declares no conflicts of interest. While the other authors declared that there are no conflicts of interest.

Ethical approval and consent to participate

Not applicable.

Consent for publication

Not applicable.

REFERENCES

1. de Langen P, Turró M, Fontanet M, Caballé J. The infrastructure investment needs and financing challenge of European ports; 2018. Available from: https://www.espo.be/media/Port%20Investment%20Study%202018_FINAL_1.pdf [Last accessed on 11 Nov 2024].
2. Lauritzen PN, Reichard J, Ahmed S, Safa M. Review of non-destructive testing methods for physical condition monitoring in the port industry. *J Constr Eng Manag Innov* 2019;2:103-11. DOI
3. Hossain NUI, Nur F, Hosseini S, Jaradat R, Marufuzzaman M, Puryear SM. A Bayesian network based approach for modeling and assessing resilience: a case study of a full service deep water port. *Reliab Eng Syst Saf* 2019;189:378-96. DOI
4. Zhang Y, Kim CW, Tee KF, Lam JSL. Optimal sustainable life cycle maintenance strategies for port infrastructures. *J Clean Prod* 2017;142:1693-709. DOI
5. Rodrigue JP. The geography of transport systems. London: Routledge; 2020. DOI
6. Negi P, Kromanis R, Dorée A, Wijnberg KM. Structural health monitoring of inland navigation structures and ports: a review on developments and challenges. *Struct Health Monit* 2023;23:147592172311707 DOI
7. Heffron RE. Waterfront facilities inspection and assessment. Reston, VA, USA: ASCE; 2015. DOI
8. Klerk WJ, Schweckendiek T, den Heijer F, Kok M. Value of information of structural health monitoring in asset management of flood defences. *Infrastructures* 2019;4:56. DOI
9. Leblouba M, Tarabin M, Zahri M. Probabilistic analysis and simulation of crack propagation in concrete pavements and surfaces. *Sci Rep* 2022;12:14157. DOI
10. Zhang Y, Lu Y, Duan Y, et al. Robust surface crack detection with structure line guidance. *Int J Appl Earth Obs Geoinf* 2023;124:103527. DOI
11. Munawar HS, Hammad AWA, Haddad A, Soares CAP, Waller ST. Image-based crack detection methods: a review. *Infrastructures* 2021;6:115. DOI
12. Gupta P, Dixit M. Image-based crack detection approaches: a comprehensive survey. *Multimed Tools Appl* 2022;81:40181-229. DOI
13. Ding W, Yang H, Yu K, Shu J. Crack detection and quantification for concrete structures using UAV and transformer. *Automat Constr* 2023;152:104929. DOI

14. Jin T, Zhang W, Chen C, Chen B, Zhuang Y, Zhang H. Deep-learning- and unmanned aerial vehicle-based structural crack detection in concrete. *Buildings* 2023;13:3114. DOI
15. Song F, Liu B, Yuan G. Pixel-level crack identification for bridge concrete structures using unmanned aerial vehicle photography and deep learning. *Struct Control Health Monit* 2024;2024:1299095. DOI
16. Li Y, Ma J, Zhao Z, Shi G. A novel approach for UAV image crack detection. *Sensors* 2022;22:3305. DOI
17. Woo HJ, Seo DM, Kim MS, Park MS, Hong WH, Baek SC. Localization of cracks in concrete structures using an unmanned aerial vehicle. *Sensors* 2022;22:6711. DOI
18. Choi D, Bell W, Kim D, Kim J. UAV-driven structural crack detection and location determination using convolutional neural networks. *Sensors* 2021;21:2650. DOI
19. Tsaimou CN, Sartampakos P, Tsoukala VK. UAV-driven approach for assisting structural health monitoring of port infrastructure. *Struct Infrastruct Eng* 2023;1-20. DOI
20. Ali R, Chuah JH, Talip MSA, Mokhtar N, Shoaib MA. Structural crack detection using deep convolutional neural networks. *Autom Constr* 2022;133:103989. DOI
21. Arvidsson B, Johansson J, Guldåker N. Critical infrastructure, geographical information science and risk governance: a systematic cross-field review. *Reliab Eng Syst Saf* 2021;213:107741. DOI
22. Lesiak P. Inspection and maintenance of railway infrastructure with the use of unmanned aerial vehicles. *Probl Kolejn* 2020;115-27. DOI
23. Li R, Yu J, Li F, Yang R, Wang Y, Peng Z. Automatic bridge crack detection using Unmanned aerial vehicle and Faster R-CNN. *Constr Build Mater* 2023;362:129659. DOI
24. Zhao Y, Zhou L, Wang X, Wang F, Shi G. Highway crack detection and classification using UAV remote sensing images based on CrackNet and CrackClassification. *Appl Sci* 2023;13:7269. DOI
25. Azouz Z, Honarvar Shakibaei Asli B, Khan M. Evolution of crack analysis in structures using image processing technique: a review. *Electronics* 2023;12:3862. DOI
26. Sundararajan D. Digital image processing: a signal processing and algorithmic approach. Singapore: Springer; 2017. DOI
27. Liu YF, Cho S, Spencer Jr. BF, Fan JS. Concrete crack assessment using digital image processing and 3D scene reconstruction. *J Comput Civ Eng* 2016;30:04014124. DOI
28. Archana R, Jeevaraj PSE. Deep learning models for digital image processing: a review. *Artif Intell Rev* 2024;57:11. DOI
29. Fan L, Zhang F, Fan H, Zhang C. Brief review of image denoising techniques. *Vis Comput Ind Biomed Art* 2019;2:7. DOI
30. Otsu N. A threshold selection method from gray-level histograms. *IEEE Trans Syst Man Cybern* 1979;9:62-6. DOI
31. Niblack W. An introduction to digital image processing. Englewood Cliffs, NJ: Prentice-Hall International; 1986. Available from: https://archive.org/details/introductiontodi0000nibl [Last accessed on 11 Nov 2024].
32. Sauvola J, Pietikäinen M. Adaptive document image binarization. *Pattern Recognit* 2000;33:225-36. DOI
33. Sobel I, Feldman G. A 3 × 3 isotropic gradient operator for image processing; 1973. Available from: https://www.researchgate.net/publication/285159837_A_33_isotropic_gradient_operator_for_image_processing [Last accessed on 11 Nov 2024].
34. Canny J. A computational approach to edge detection. *IEEE Trans Pattern Anal Mach Intell* 1986;PAMI-8:679-98. DOI
35. Dorafshan S, Maguire M, Qi X. Automatic surface crack detection in concrete structures using OTSU thresholding and morphological operations. UTC Report 01-2016. Utah State University; 2016. DOI
36. Kim IH, Jeon H, Baek SC, Hong WH, Jung HJ. Application of crack identification techniques for an aging concrete bridge inspection using an unmanned aerial vehicle. *Sensors* 2018;18:1881. DOI
37. Li H, Wang W, Wang M, Li L, Vimlund V. A review of deep learning methods for pixel-level crack detection. *J Traffic Transp Eng* 2022;9:945-68. DOI
38. Jofré-Briceño C, Muñoz-La Rivera F, Atencio E, Herrera RF. Implementation of facility management for port infrastructure through the use of UAVs, photogrammetry and BIM. *Sensors* 2021;21:6686. DOI
39. Harris DK, Brooks CN, Ahlborn TM. Synthesis of field performance of remote sensing strategies for condition assessment of in-service bridges in Michigan. *J Perform Constr Facil* 2016;30:04016027. DOI
40. GDAL/OGR geospatial data abstraction software library; 2024. DOI
41. Rasterio/affine's documentation; 2024. Available from: https://affine.readthedocs.io/en/latest/ [Last accessed on 11 Nov 2024].
42. Chen C, Seo H, Jun C, Zhao Y. A potential crack region method to detect crack using image processing of multiple thresholding. *Signal Image Video Process* 2022;16:1673-81. DOI
43. Chityala R, Pudipeddi S. Image processing and acquisition using Python. 2nd ed. Boca Raton: Chapman and Hall/CRC Press; 2020. p. 452. DOI
44. Owotogbe JS, Ibiyemi TS, Adu BA. A comprehensive review on various types of noise in image processing. *Int J Sci Eng Res* 2019;10:388-93. Available from: https://www.ijser.org/researchpaper/A-COMPREHENSIVE-REVIEW-ON-VARIOUS-TYPES-OF-NOISE-IN-IMAGE-PROCESSING.pdf [Last accessed on 11 Nov 2024].
45. Gonzalez RC, Woods RE. Digital image processing. 4th ed. Essex, England: Pearson Education Limited; 2018. Available from: https://dl.icdst.org/pdfs/files4/01c56e081202b62bd7d3b4f8545775fb.pdf [Last accessed on 11 Nov 2024].
46. Xu B, Chen J, Yu P. Vectorization of classified remote sensing raster data to establish topological relations among polygons. *Earth Sci Inform* 2017;10:99-113. DOI
47. Zhang F, Hu Z, Yang K, Fu Y, Feng Z, Bai M. The surface crack extraction method based on machine learning of image and quantitative feature information acquisition method. *Remote Sens* 2021;13:1534. DOI
48. Obi JC. A comparative study of several classification metrics and their performances on data. *World J Adv Eng Technol Sci* 2023;8:308-14.

DOI

49. Tharwat A. Classification assessment methods. *Appl Comput Inform* 2020;17:168-92. DOI
50. Yang YS, Wu Cl, Hsu TTC, Yang HC, Lu HJ, Chang CC. Image analysis method for crack distribution and width estimation for reinforced concrete structures. *Autom Constr* 2018;91:120-32. DOI
51. Feng K, Ji JC, Ni Q, Li Y, Mao W, Liu L. A novel vibration-based prognostic scheme for gear health management in surface wear progression of the intelligent manufacturing system. *Wear* 2023;522:204697. DOI
52. Feng K, Ni Q, Chen Y, Ge J, Liu Z. A cyclostationarity-based wear monitoring framework of spur gears in intelligent manufacturing systems. *Struct Health Monit* 2023;22:147592172211470. Available from: https://www.researchgate.net/publication/367100031_A_cyclostationarity-based_wear_monitoring_framework_of_spur_gears_in_intelligent_manufacturing_systems [Last accessed on 11 Nov 2024].